Measurements of electron–phonon coupling factor and interfacial thermal resistance of metallic nano-films using a transient thermoreflectance technique*

Wang Hai-Dong(王海东)[a], Ma Wei-Gang(马维刚)[a], Guo Zeng-Yuan(过增元)[a], Zhang Xing(张 兴)[a]†, and Wang Wei(王 玮)[b]

[a] *Key Laboratory for Thermal Science and Power Engineering of Ministry of Education, Department of Engineering Mechanics, Tsinghua University, Beijing* 100084, *China*

[b] *Institute of Microelectronics, Peking University, Beijing* 100871, *China*

(Received 27 August 2010; revised manuscript received 26 October 2010)

Using a transient thermoreflectance (TTR) technique, several Au films with different thicknesses on glass and SiC substrates are measured for thermal characterization of metallic nano-films, including the electron–phonon coupling factor G, interfacial thermal resistance R, and thermal conductivity K_s of the substrate. The rear heating-front detecting (RF) method is used to ensure the femtosecond temporal resolution. An intense laser beam is focused on the rear surface to heat the film, and another weak laser beam is focused on the very spot of the front surface to detect the change in the electron temperature. By varying the optical path delay between the two beams, a complete electron temperature profile can be scanned. Different from the normally used single-layer model, the double-layer model involving interfacial thermal resistance is studied here. The electron temperature cooling profile can be affected by the electron energy transfer into the substrate or the electron–phonon interactions in the metallic films. For multiple-target optimization, the genetic algorithm (GA) is used to obtain both G and R. The experimental result gives a deep understanding of the mechanism of ultra-fast heat transfer in metals.

Keywords: transient thermoreflectance technique, electron–phonon coupling factor, interfacial thermal resistance, genetic algorithms

PACS: 07.20.–n, 42.60.By, 63.20.kd **DOI:** 10.1088/1674-1056/20/4/040701

1. Introduction

The development of metallic nano-film processing in advanced micro-electronic devices highlights considerable needs for thermal characterization.[1] Especially when combined with the ultra-fast laser processing technique, the quantitative determination of ultra-fast electron–phonon interactions becomes a problem of great concern.[2,3] Some researchers have reported on the new micro-structures formed in glass or alloys by femtosecond laser processing,[4,5] so the deep understanding of the ultra-fast heat transfer in materials is required in particular. Because the time needed for electrons and phonons to reach a thermal equilibrium state is only several picoseconds, a transient measurement technique with ultra-high time resolution should be developed. On the other hand, the interfacial thermal resistance is commonly considered as a major factor in restraining the overall performance of the electric devices. The measurement of the interfacial thermal resistance is already an important part of the thermal characterization of metallic films.[6] To develop the performance of the micro-electronic devices, both electron–phonon coupling and interfacial thermal resistance should be taken into account, especially for treating the metallic nano-films. However, the normally used thermosensible electrical resistance methods cannot be used to study the transient thermal properties of metallic films because of their low temporal resolution. Also, they are not suitable for measuring the interfacial thermal resistance between the nano-film and the dielectric substrate under transient laser heating conditions.[7–9] To solve this problem, we have built a femtosecond transient thermoreflectance (TTR) system for measuring the transient electron temperature responses to obtain both the coupling factor and the interfacial thermal resistance. By using the optical pump-probe technique, a femtosecond time resolution can be achieved.

*Project supported by the National Natural Science Foundation of China (Grant Nos. 50730006, 50976053, and 50906042).

†Corresponding author. E-mail: x-zhang@tsinghua.edu.cn

© 2011 Chinese Physical Society and IOP Publishing Ltd

2. Transient thermoreflectance experimental system

The femtosecond transient thermoreflectance technique has been demonstrated as an effective way to study ultra-fast heat transfer in materials.[10] It has been successfully used to study the rate of coupling between electrons and phonons in metallic films and to determine the thermal properties of films on a femtosecond time scale.[11] In our experiments, an intense pump laser beam is focused on the rear surface to heat the film sample. Meanwhile, another weak probe laser beam is focused on the front surface to monitor the change in the reflectance, which represents the instantaneous electron temperature change. The experimental setup is shown in Fig. 1.

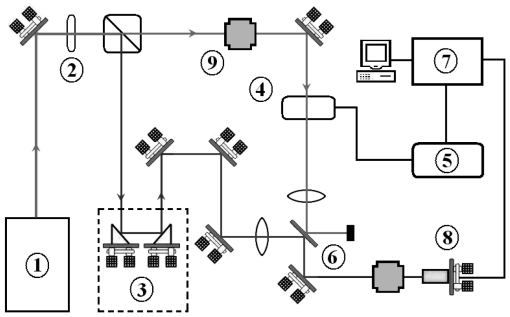


Fig. 1. Experimental setup of femtosecond laser pump-probe system. 1: Femtosecond laser, 2: wave plate, 3: optical path delay, 4: acousto-optic modulator, 5: signal generator, 6: sample, 7: lock-in amplitier, 8: photodetector, 9: calcite polarizer.

The laser pulses from a MaiTai titanium:sapphire laser are generated at 80 MHz and then separated into two beams by a polarizing beam splitter. One intense beam ($\sim$ 3.75 nJ/pulse) is used to heat the metallic film, which is referred to as the pump beam. The other weak beam ($\sim$ 0.15 nJ/pulse) is used to detect the change in reflectivity, which is referred to as the probe beam. The probe beam is focused on the front surface of the film to detect the TTR signal responses while the same spot on the rear surface is heated by the pump beam. The electron temperature profile is scanned by changing the optical path delay between the pump beam and the probe beam step-by-step. The lock-in amplification technique is used in the experiments to monitor the weak TTR signals. The pump beam passes through an acousto-optic modulator (AOM), creating a modulated pulse train at a prescribed frequency of 1 MHz. Then a series of heating events at the modulated frequency are created when the pump beam reaches the film surface. The optical path delay is precisely controlled by a stepping motor. The time delay is 6.7 fs as the stepping motor moves 1 μm. The reflected probe beam is sent into a photodiode detector, which provides a measurable voltage signal. Then the signal is collected by a lock-in amplifier according to the modulated frequency of AOM. There is a pair of calcite polarizers placed in the pump beam path and the probe beam path separately. The first polarizer is used to rotate the polarization of the pump beam, making it perpendicular to the polarization of the probe beam. The second polarizer placed in front of the detector is used to reduce the noise caused by the scattered pump light.

Table 1. Experimental conditions.

parameter	specification
wavelength	800 nm
modulated frequency	1.0 MHz
maximum pump laser power	300 mW
probe laser power	< 15 mW
focal spot diameter	100 μm
resolution of stepping motor	8.5 nm

Table 1 summarizes the experimental conditions of the femtosecond laser pump-probe system.

In 1974, Anisimov *et al.*[12] developed a two-temperature model to describe the heat transfer during ultra-fast laser heating in metals. This model is on the assumption that the "hot" electrons transfer the absorbed energy to the "cold" lattices through electron–phonon collisions. There are established two temperature systems (electron temperature $T_{\rm e}$ and lattice temperature $T_{\rm l}$) in this transient non-equilibrium heat transfer process. The change in the reflectivity of the metal is related to the change in the complex dielectric constant that is a function of frequency and temperature, i.e., $\Delta\varepsilon(\omega, \Delta T) = \Delta\varepsilon_1(\omega, \Delta T) + {\rm i}\,\Delta\varepsilon_2(\omega, \Delta T)$, where ε_1 and ε_2 are the real and the imaginary parts of the dielectric constant, respectively.[13] Then the change in reflectivity can be expressed as

$$\frac{\Delta R_f}{R_f} = \frac{1}{R_f}\left[\frac{\partial R_f}{\partial \varepsilon_1}\Delta\varepsilon_1 + \frac{\partial R_f}{\partial \varepsilon_2}\Delta\varepsilon_2\right]. \tag{1}$$

When the change in the electron temperature is small, ($\Delta T_{\rm e} < 150$ K) as in our experiments, $\Delta\varepsilon$ can be expressed in a total differential form as[14–16]

$$\Delta\varepsilon = \frac{\partial\varepsilon_1}{\partial T_{\rm e}}\Delta T_{\rm e} + \frac{\partial\varepsilon_1}{\partial T_{\rm l}}\Delta T_{\rm l} + {\rm i}\left(\frac{\partial\varepsilon_2}{\partial T_{\rm e}}\Delta T_{\rm e} + \frac{\partial\varepsilon_2}{\partial T_{\rm l}}\Delta T_{\rm l}\right). \tag{2}$$

Combining Eq. (1) with Eq. (2), the change in reflectivity can be simplified to[14]

$$\frac{\Delta R_f}{R_f} = a\Delta T_{\rm e} + b\Delta T_{\rm l}, \tag{3}$$

where a and b are the constant coefficients for electron temperature and lattice temperature, respectively. The change in the lattice temperature can be neglected in our experiments, thus the change in the reflectivity is proportional to the change in the electron temperature, as

$$\frac{\Delta R_f}{R_f} = a\Delta T_{\rm e}. \tag{4}$$

In our experiments, different metallic films are prepared on 500-μm borosilicate glass and 100-nm SiC substrate using a physical vapour deposition method. The surface of the film sample is scanned using an atomic force microscope (AFM). The resulting image is shown in Fig. 2.

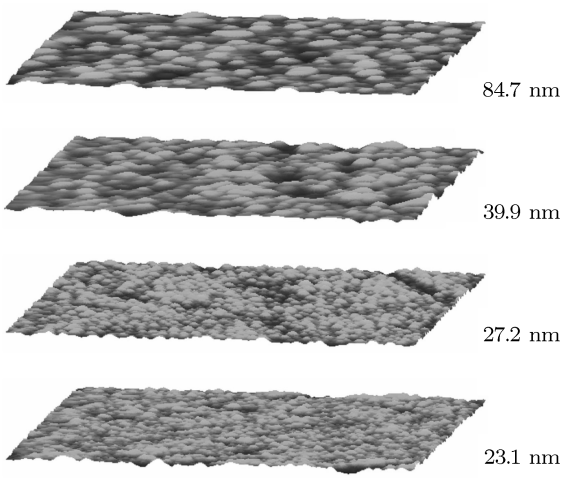


Fig. 2. Different Au films with thicknesses of 84.7, 39.9, 27.2 and 23.1 nm, scanned using AFM. The grain size of the film is evaluated for experimental data analysis.

The measured average gain sizes in different Au films are listed in Table 2.

Table 2. Measured average grain sizes in Au films.

film thickness/nm	23.1	27.2	39.9	84.7
average grain size/nm	15	23	30	49

It is noted that the grain size increases as the film thickness increases. The smoothness of the film surface may affect the measured TTR signals.

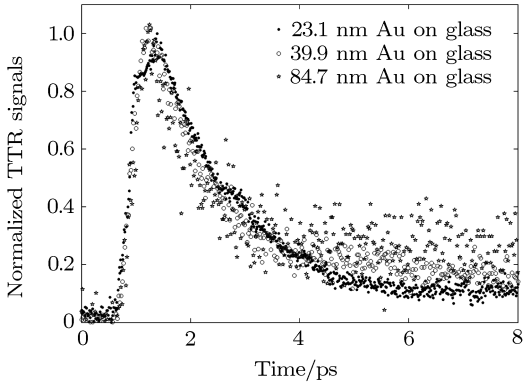


Fig. 3. TTR signal profiles of different film thicknesses on glass substrate, measured using the femtosecond laser pump-probe system. TTR signals represent the change in the electron temperature. The electron temperature profiles can be used for fitting the thermal properties.

It is observed that the measured TTR signal amplitude decreases as the film thickness increases. There are two possible reasons: 1) the electron temperature decreases when the energy is transferred through the thicker films; 2) the rough film surface weakens the TTR signals, and the larger grain size in thicker film leads to the smaller TTR signal amplitude.

It is observed in Fig. 4 that the electron temperature profile of Au film on SiC is lower than that on glass substrate, while the two film thicknesses are almost the same. This indicates that the difference in substrate will affect the electron temperature cooling curve. As a result, the metallic film cannot be treated with a single-layer model. A double-layer model involving interfacial thermal resistance should be used instead.

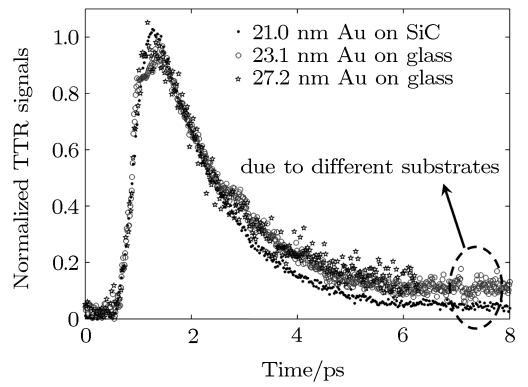


Fig. 4. TTR signal profiles of Au films on different substrates. The different normalized electron temperature responses on glass and SiC substrates can be compared. It is seen that the electron energy is easier to transfer to the SiC substrate than to the thermally insulative glass substrate.

3. Mathematical models

Qui and Tien[17] proposed a microscopic parabolic two-step (PTS) model to predict the temperature response after femtosecond laser heating. The complete PTS model is given as

$$C_{\rm e}\frac{\partial T_{\rm e}}{\partial t} = \frac{\partial}{\partial x}\left(k_{\rm e}\frac{\partial T_{\rm e}}{\partial x}\right) - G(T_{\rm e}-T_0) + S, \quad (5)$$

$$C_{\rm l}\frac{\partial T_{\rm l}}{\partial t} = G\left(T_{\rm e}-T_{\rm l}\right), \quad (6)$$

where C, T, k, G and S are the specific heat, temperature, thermal conductivity, electron–phonon coupling factor and laser source term, respectively. The subscripts e and l represent the electron and lattice, respectively. $k_{\rm e}$ is actually the efficient electron thermal conductivity induced by e–e and e–l scatterings, defined as $k_{\rm e} = k_0\ (T_{\rm e}/T_{\rm l})$.[18] This expression for conductivity is valid for relatively low electron temperature, as in our experiments. The Gaussian laser heating source term S in the governing equation is expressed as[19,20]

$$S(x,t) = \sqrt{4\ln 2}\frac{(1-R_f)J}{\tau_{\rm p}\delta\sqrt{\pi}} \times \exp\left(-\frac{x}{\delta} - 4\ln 2\left(\frac{t-2\tau_{\rm p}}{\tau_{\rm p}}\right)^2\right), \quad (7)$$

where $R_{\rm f}$ is the reflectivity of the film, δ is the radiation penetration depth, and J is the laser pulse intensity. In our experiments, J is about 0.96 J·m^{-2} and the corresponding maximum electron temperature rise is below 100 K. In addition, the corresponding maximum lattice temperature rise is below 1 K in the initial stage of heating. As mentioned above, the film is normally treated as a single-layer with two thermal insulation boundaries (see Fig. 5(b)).[21] But due to our experimental observation in Fig. 4, a double-layer model should be considered here.

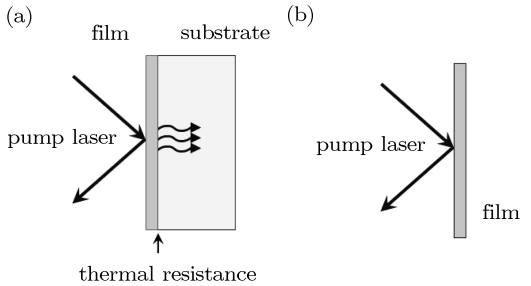


Fig. 5. (a) Double-layer model, which takes the interfacial thermal resistance into account, by which the substrate-dependent effect can be studied, and (b) single-layer model with two thermal insulation boundaries, and the electron temperature is affected only by electron–phonon interaction.

The heat leak from the hot electrons into the substrate is considered as the interfacial thermal resistance in the double-layer model. The interfacial boundary conditions are given as

$$-k_{\rm e}\frac{\partial T_{\rm e}}{\partial x}\bigg|_{x=d} = -k_{\rm s}\frac{\partial T_{\rm s}}{\partial x}\bigg|_{x=d}, \quad (8)$$

$$-k_{\rm e}\frac{\partial T_{\rm e}}{\partial x}\bigg|_{x=d} = \frac{T_{\rm e}-T_{\rm s}}{R}\bigg|_{x=d}, \quad (9)$$

where $x = d$ is the interface between the film and the substrate. $k_{\rm s}$, $T_{\rm s}$ and R are the substrate thermal conductivity, substrate temperature and electron–substrate interfacial thermal resistance, respectively. A semi-implicit Crank–Nicholson scheme is used to solve the PTS governing equations. The convergence criterion of the calculation is set to be $\Delta T_{\rm e}/T_{\rm e} < 10^{-8}$ for each time step. A uniform grid system is used with 400 grid points and the time step is chosen to be 5 fs. Furthermore, different grid spacings and time steps are used to check the consistency and stability of the numerical solutions.

As shown in Fig. 6, the interfacial condition will affect the rate of cooling the hot electrons in the metallic film. It should be mentioned that R is actually the electron–substrate interfacial thermal resistance describing the transient heat loss from the electrons to the substrate. Chen *et al.*[22] proposed a temperature-dependent model for G, indicating that G increases as the electron temperature increases. The smaller R decreases the electron temperature, leading to a decreased G. As a result, the single-layer model will over-estimate the coupling factor G, which is actually an apparent electron–phonon coupling factor, as discussed in Ref. [13]. In a three-temperature model proposed by Hopkins and Norris,[23] the cooling of the electrons is contributed by both electron–phonon coupling and electron–substrate energy transfer. From another point of view, some researchers[24,25] pointed out that the transient energy transfer from the electrons to the substrate is possible by coupling between electrons and phonons within the metal, and then subsequently coupling between the phonons in the metal and the phonons in the substrate. It is noteworthy that the electron–phonon coupling is part of the interfacial thermal conductance. In the experimental data analysis, we use a genetic algorithm (GA) method to

determine R and G simultaneously.

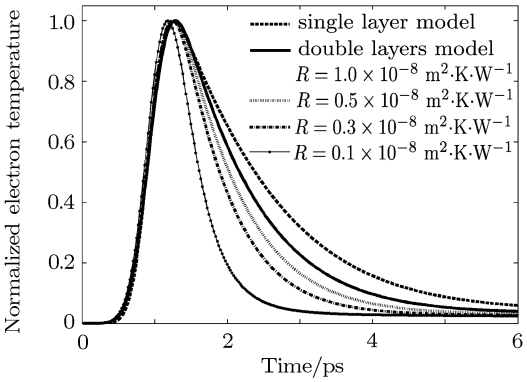


Fig. 6. Comparison between electron temperature profiles obtained based on the single-layer model and the double-layer model for different R values showing that the smaller interfacial thermal resistance leads to a lower electron temperature cooling curve. The substrate-dependent effect should be attributed to the electron–phonon interaction in the metallic film.

4. Experimental data analysis

The objective function S is given as

$$S = \sum_{i=1}^{N} \left[\tilde{\theta}_i(t) - \theta_i(t)\right]^2,$$

where $\tilde{\theta}(t)$ and $\theta(t)$ are the measured and the calculated normalized temperatures, respectively. The minimum function S gives the best fitting to the measured temperature curve, and so the thermal parameters can be obtained. In order to verify the accuracy of the GA method, we give the true thermal properties as electron–phonon coupling factor $G = 2.5 \times 10^{16}$ W·m^{-3}·K^{-1} and interfacial thermal resistance $R = 1.0 \times 10^{-8}$ m^2·K·W^{-1}. Then the GA simulation is repeated 5 times and the results are shown in Table 3.

Table 3. Results of GA simulation.

No.	1	2	3	4	5	average
$G/10^{-16}$ W·m^{-3}·K^{-1}	2.47	2.47	2.57	2.56	2.57	2.53
$R/10^{8}$ m^2·K·W^{-1}	0.80	0.81	1.1	1.1	0.78	0.92

The GA simulation uncertainties of G and R are 1.2% and 8.0%, respectively.

The sensitivity analysis in Fig. 7 reveals that the larger deviation in R from the its average value is due to its lower sensitivity.

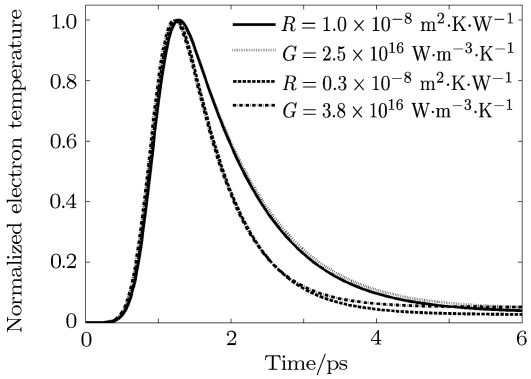
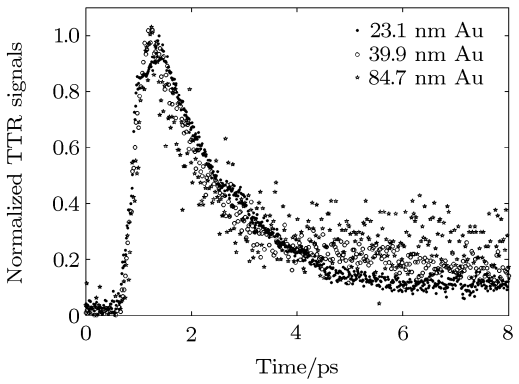
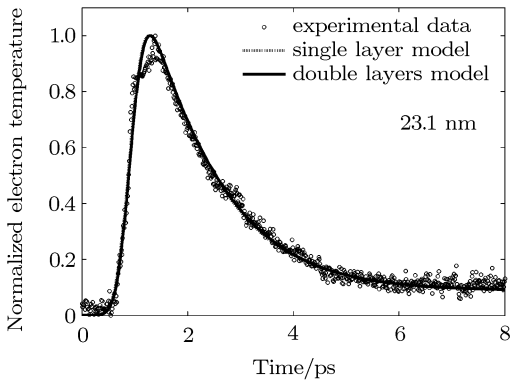


Fig. 7. Numerical simulation results, showing that the 52% increase in G is comparable to a 70% decrease in R, which indicates that G is more sensible to the measured electron temperature profile.

4.1. Measurements of nano-films with different thicknesses

As shown in Fig. 8, the calculated profiles based on two models are compared with the experimental data for different thicknesses.





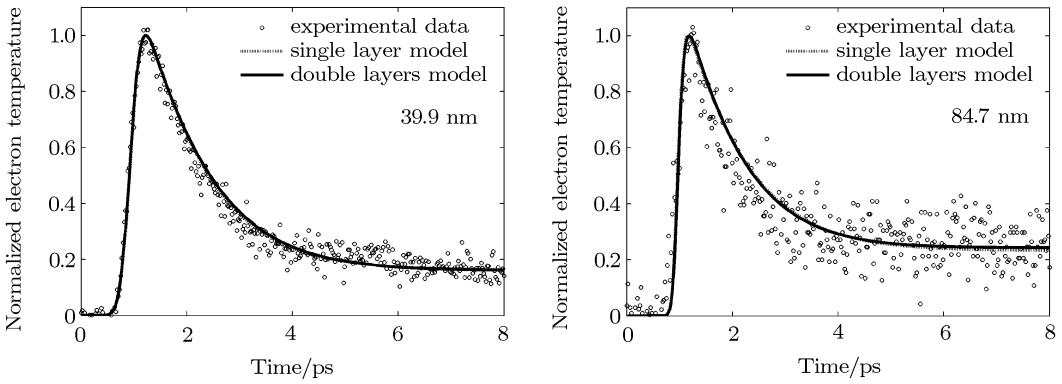


Fig. 8. Comparison between measured TTR data and normalized electron temperature profiles calculated using G and R selected by the GA method based on the single-layer model and double-layer model.

The electron thermal conductivity, the electron specific heat, and the lattice specific heat of Au are calculated to be $k_{\rm e} = k_0 T_{\rm e}/T_{\rm l}$ ($k_0 = 315$ W·m^{-1}·K^{-1}), $C_{\rm e} = A_{\rm e} T_{\rm e}$ ($A_{\rm e} = 70$ J·m^{-3}·K^{-2}) and $C_{\rm l} = 2.5 \times 10^6$ J·m^{-3}·K^{-1}, respectively.[17] Due to our numerical results, the predicted electron temperature profiles are insensitive to the electron thermal conductivity and thus the bulk value is acceptable. The bulk specific heat and the bulk thermal conductivity of the borosilicate glass are calculated to be 1.73×10^6 J·m^{-3}·K^{-1} and 1.10 W·m^{-1}·K^{-1}, respectively. The estimated G and R for different film thicknesses are listed in Table 4.

Table 4. Results of GA simulation for different Au films.

No.	parameters	23.1 nm	39.9 nm	84.7 nm
1	$G/10^{-16}$ W·m^{-3}·K^{-1}	1.7394	1.9727	2.0869
	$R/10^8$ m^2·K·W^{-1}	5.91	12.88	29.80
2	$G/10^{-16}$ W·m^{-3}·K^{-1}	1.7394	1.9020	1.8606
	$R/10^8$ m^2·K·W^{-1}	5.64	18.82	21.82
3	$G/10^{-16}$ W·m^{-3}·K^{-1}	1.7333	2.0434	1.9657
	$R/10^8$ m^2·K·W^{-1}	5.73	17.83	24.85
4	$G/10^{-16}$ W·m^{-3}·K^{-1}	1.7273	2.1000	1.9899
	$R/10^8$ m^2·K·W^{-1}	5.36	16.84	27.58
5	$G/10^{-16}$ W·m^{-3}·K^{-1}	1.7455	1.9727	2.2000
	$R/10^8$ m^2·K·W^{-1}	5.82	12.88	23.94
average	$G/10^{-16}$ W·m^{-3}·K^{-1}	1.74	2.00	2.02
	$R/10^8$ m^2·K·W^{-1}	5.69	15.85	25.60

Meanwhile, based on the single-layer model, the apparent coupling factors of 23.1 nm, 39.9 nm and 84.7 nm films are determined to be 1.95×10^{16} W·m^{-3}·K^{-1}, 2.10×10^{16} W·m^{-3}·K^{-1} and 2.20×10^{16} W·m^{-3}·K^{-1}, respectively. The results are summarized in Fig. 9.

Qiu and Tien[26] studied the non-equilibrium heat conduction in metals and developed a simple thermodynamic expression as

$$G = \frac{9}{16}\frac{nk^2 T_D^2 v_{\rm F}}{\Lambda T_{\rm l} E_{\rm F}}, \tag{10}$$

where Λ is the effective electron mean free path in polycrystalline thin film. n, k, $T_{\rm D}$, $v_{\rm F}$ and $E_{\rm F}$ are the electron number density, Boltzmann constant, Debye temperature, Fermi velocity and Fermi energy, respectively. The bulk value of the coupling factor is calculated to be 2.3×10^{16} W·m^{-3}·K^{-1}, which is slightly larger than the simulation results.

Majumdar and Reddy[24] proposed a physical model to describe the energy transfer from electrons to substrate as

$$R = \frac{1}{\sqrt{Gk_{\rm l}}} + R_{\rm ps} = R_{\rm ep} + R_{\rm ps};\ R_{\rm ep} = \frac{1}{\sqrt{Gk_{\rm l}}}, \tag{11}$$

where $R_{\rm ep}$ and$R_{\rm ps}$ are the electron–phonon thermal resistance in metals and the phonon–substrate thermal resistance through the interface. It is noted that the interfacial thermal resistance R is the sum of these

two thermal resistances. Based on the measured G in Fig. 9, R_{ep} is found to be about 0.3×10^{-8} m^2·K·W^{-1}, which is within 10% of the measured R. This suggests that the most interfacial thermal conductance is contributed by the phonon–substrate coupling at the metal–nonmetal interface and the measured R (5×10^{-8} m^2·K·W^{-1} ~26×10^{-8} m^2·K·W^{-1}) is close to the other GA simulation results of Au films on SiO_2 substrates.[27] The fact that the measured R increases as the film thickness increases in Fig. 9 may be due to the roughness of the surface and the thermal stress in the film. The surface roughness may increase as the grain size increases, as shown in Table 2. This is also proved by the fact that the noise induced by the scattered pump light increases as the film becomes thicker. The increasing roughness will lead to a larger R_{ps} as the film thickness increases.[28] Secondly, the thermal stress in the metallic film is proportional to the metal layering time, and more thermal stress, i.e. thicker metallic film, will cause a larger interfacial thermal resistance.[29]

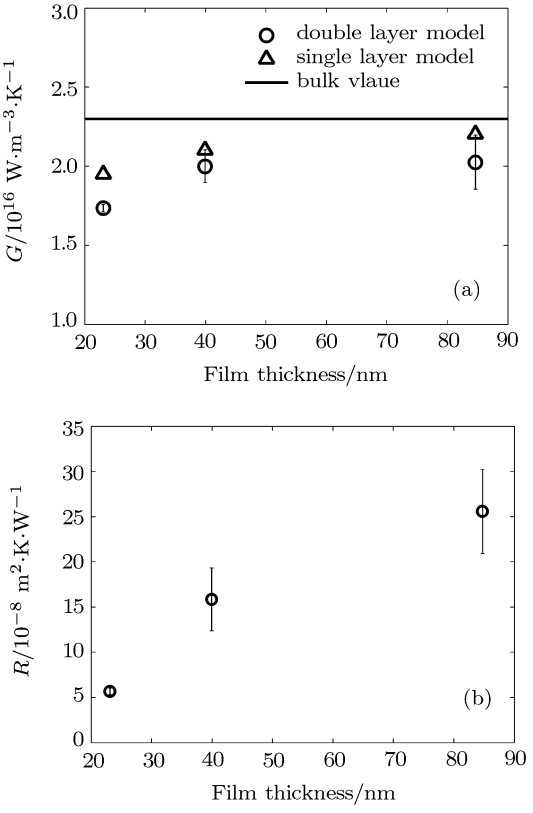


Fig. 9. The best-fitting G based on the single-layer model is larger than that based on the double-layer model, because the electron energy transferred into the substrate is considered as a part of G in the single-layer model (a); R increasing as the film thickness increases (b).

4.2. Measurements of nano-films with different substrates

It is noted that the cooling curve on the SiC substrate is lower than that on the glass substrate in Fig. 10. This substrate-dependent feature is confirmed by the repeated measurements of 23.1 nm and 27.2 nm Au films on the glass substrates. Because the thermal conductivity of 100-nm SiC film may be different from the bulk value, we choose G, R and SiC thermal conductivity k_s as the objective parameters for the GA simulation. The best-fitting values after 5 runs are $G = 1.93\times10^{16}$ W·m^{-3}·K^{-1}, $R = 11.14\times10^{-8}$ m^2·K·W^{-1}, and $K_s = 131.30$ W·m^{-1}·K^{-1}. The best-fitting profile using these parameters is also plotted in Fig. 10. It is seen that the energy of the electrons is more readily transferred to the SiC substrate than to the thermally insulating glass substrate, and the Au–SiC coupling factor is larger than the Au-glass coupling factor 1.74×10^{16} W·m^{-3}·K^{-1} for 23.1-nm film. This substrate dependence of G is more significant when the film is heated by higher power laser beams, as discussed in Ref. [13].

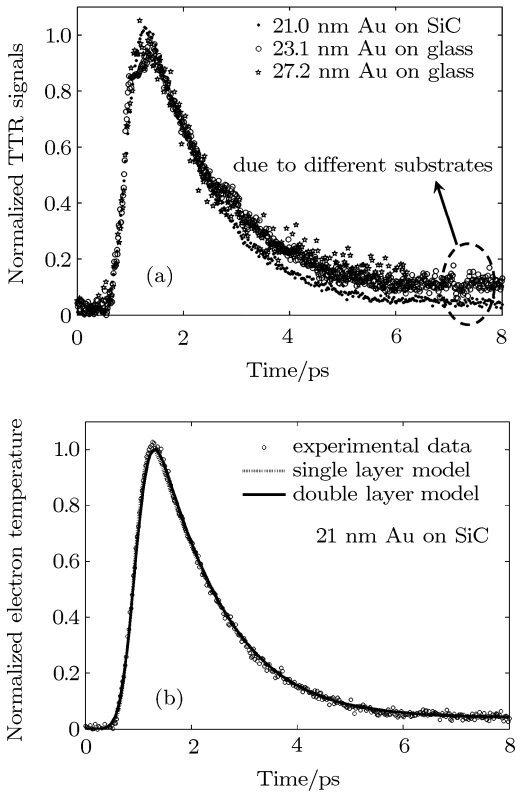


Fig. 10. Comparison between TTR data measured and calculated based on two models (a), and normalized electron temperature profiles on SiC substrate and glass substrate, showing that the former is lower than the latter.

5. Conclusions

The non-equilibrium electron–phonon interactions and interfacial thermal resistance are two major concerns in studying the transient heat conduction induced by the ultra-fast laser heating. We have built a TTR system to measure the electron temperature responses of Au nano-films with different thicknesses and substrates. Unlike the normally used single-layer model, the double-layer model separates the electron–substrate cooling effect from the electron–phonon coupling effect, giving a deep understanding of the transient heat transfer mechanism. A GA method is used for the experimental data analysis. It is noted that the measured electron–phonon coupling factor accords with the theoretical prediction. The measured interfacial thermal resistance increases as the film thickness increases, owing to the increasing roughness and more thermal stress gained in the film. It is also observed in the experiment that the electron energy is more readily transferred to the SiC substrate than to the thermally insulating glass substrate because of the higher thermal conductivity of SiC and stronger interfacial electron–phonon interactions.

References

[1] Smith A N and Calame J P 2004 *Int. J. Thermophys.* **25** 409

[2] Majumdar A, Fushinobu K and Hijikata K 1995 *J. Appl. Phys.* **77** 6686

[3] Stoner R J and Maris H J 1993 *Phys. Rev.* B **48** 16373

[4] Sun H Y, Luo F F, He F, Liao Y and Xu J 2010 *Chin. Phys.* B **19** 054210

[5] Ran L L, Qu S L and Guo Z Y 2010 *Chin. Phys.* B **19** 034204

[6] Stevens R J, Smith A N and Norris P M 2005 *J. Heat Transfer* **127** 315

[7] Lee S M and Cahill D G 1997 *J. Appl. Phys.* **81** 2590

[8] Lambropoulos J C 1989 *J. Appl. Phys.* **66** 4230

[9] Orain S, Scudeller Y and Brousse T 1999 *Int. J. Thermal Sci.* **39** 537

[10] Norris P M, Caffrey A P, Stevens R J, Klopf J M, McLeskey J T and Smith A N 2003 *Rev. Sci. Instrum.* **74** 400

[11] Hopkins P E, Kassebaum J L and Norris P M 2009 *J. Appl. Phys.* **105** 023710

[12] Anisimov S I, Kapeliovich B L and Perelman T L 1974 *Sov. Phys. –JETP* **39** 375

[13] Rosei R and Lynch D W 1972 *Phys. Rev.* B **5** 3883

[14] Norris P M, Caffrey A P, Stevens R J, Klopf J M, McLeskey J T and Smith A N 2003 *Rev. Sci. Instrum.* **74** 400

[15] Brorson S D, Kazeroonian A, Moodera J S, Face D W, Cheng T K, Ippen E P, Dresselhaus M S and Dresselhaus G 1990 *Phys. Rev. Lett.* **64** 2172

[16] Hirori H, Tachizaki T, Matsuda O and Wright O B 2003 *Phys. Rev.* B **68** 113102

[17] Qiu T Q and Tien C L 1994 *Int. J. Heat Mass Transfer* **37** 2789

[18] Anisimov S I and Rethfeld B 1997 *Nonresonant Laser-Matter Interaction (NLMI-9)* **3093** 192

[19] Tang D W and Araki N 1996 *J. Phys.* D: *Appl. Phys.* **29** 2527

[20] Chen J K, Tzou D Y and Beraun J E 2006 *Int. J. Heat Mass Transfer* **49** 307

[21] Smith A N, Hostetler J L and Norris P M 1999 *Numer. Heat Transfer* A **35** 859

[22] Chen J K, Latham W P and Beraun J E 2005 *J. Laser Appl.* **17** 63

[23] Hopkins P E and Norris P M 2007 *Appl. Surf. Sci.* **253** 6289

[24] Majumdar A and Reddy P 2004 *Appl. Phys. Lett.* **84** 4768

[25] Roukes M L, Freeman M R, Germain R S, Richardson R C and Ketchen M B 1985 *Phys. Rev. Lett.* **55** 422

[26] Qiu T Q and Tien C L 1993 *J. Heat Transf. Trans. ASME* **115** 842

[27] Orain S, Scudeller Y, Garcia S and Brousse T 1999 *Int. J. Heat Mass Transfer* **44** 3973

[28] Sahling S, Engert J, Gladun A and Knoner R 1981 *J. Low Temp. Phys.* **45** 457

[29] Sakami D, Lahmar A, Scudeller Y, Danes F and Bardon J P 2001 *J. Adhesion Sci. Technol.* **15** 1403